Editors' Suggestion

Strong Interminivalley Scattering in Twisted Bilayer Graphene Revealed by High-Temperature Magneto-Oscillations

I. Y. Phinney,[1] D. A. Bandurin,[1,*] C. Collignon,[1] I. A. Dmitriev,[2,3] T. Taniguchi,[4] K. Watanabe,[5] and P. Jarillo-Herrero[1,†]

[1]*Massachusetts Institute of Technology, Cambridge, Massachusetts 02139, USA*
[2]*Physics Department, University of Regensburg, 93040, Regensburg, Germany*
[3]*Ioffe Institute, 194021 St. Petersburg, Russia*
[4]*International Center for Materials Nanoarchitectonics, National Institute of Material Science, Tsukuba 305-0044, Japan*
[5]*Research Center for Functional Materials, National Institute of Material Science, Tsukuba 305-0044, Japan*

(Received 14 April 2021; accepted 29 June 2021; published 30 July 2021)

Twisted bilayer graphene (TBG) provides an example of a system in which the interplay of interlayer interactions and superlattice structure impacts electron transport in a variety of nontrivial ways and gives rise to a plethora of interesting effects. Understanding the mechanisms of electron scattering in TBG has, however, proven challenging, raising many questions about the origins of resistivity in this system. Here we show that TBG exhibits high-temperature magneto-oscillations originating from the scattering of charge carriers between TBG minivalleys. The amplitude of these oscillations reveals that interminivalley scattering is strong, and its characteristic timescale is comparable to that of its intraminivalley counterpart. Furthermore, by exploring the temperature dependence of these oscillations, we estimate the electron-electron collision rate in TBG and find that it exceeds that of monolayer graphene. Our study demonstrates the consequences of the relatively small size of the superlattice Brillouin zone and Fermi velocity reduction on lateral transport in TBG.

DOI: 10.1103/PhysRevLett.127.056802

Two graphene monolayers, placed on top of each other with a small rotational misalignment between their crystallographic axes, form a long-wavelength moiré superlattice. The electronic properties of such a superlattice depend on the relative twist angle θ between the graphene layers as well as their interlayer hybridization. A particularly interesting case is that of small-angle ($\theta < 3°$) TBG (SA TBG), where hybridization is strong, and which, for a certain range of angles, features intriguing interaction-driven phenomena including, but not limited to, superconductivity [1,2], correlated insulator states [3], and orbital ferromagnetism [4,5]. The low-energy single-particle band structure of SA TBG resembles that of monolayer graphene (MLG) but is characterized by a decreased Fermi velocity v_F and a reduced Brillouin zone (BZ) [6]. Like the BZ of MLG, the reduced BZ is hexagonal and contains two minivalleys located at the k_m and k'_m high-symmetry points [7]. The minivalleys are spaced apart by a relatively small (in comparison to MLG) distance, $\Delta k = (4\pi/a)\sin(\theta/2)$, where a is the lattice constant of MLG [Fig. 1(a)]. In MLG, the intervalley separation is sufficiently large so as to suppress intervalley electron scattering, provided that atomically sharp defects are absent [8]. In this work, we show that the opposite is true for SA TBG, where strong interminivalley scattering significantly affects its transport properties.

Our devices are multiterminal Hall bars composed of SA TBG encapsulated between two relatively thin (< 100 nm thick) slabs of hexagonal boron nitride (h-BN). The Hall bars were produced by a combination of tear-and-stack [9,10] and hot-release [11] methods, were endowed with quasi-one-dimensional contacts [12], and had a typical width of about 2 μm as shown in Fig. 1(b) (see Supplemental Material [13]). Figure 1(c) shows a typical dependence of the longitudinal resistivity ρ_{xx} versus the externally induced total carrier density n, measured in one of our devices at two representative temperatures T. At small n, the $\rho_{xx}(n)$ dependence resembles that of MLG: namely, it exhibits a sharp peak of about 2 kΩ at the charge neutrality point, which rapidly drops to 20–50Ω with increasing $|n|$. Upon further doping, $\rho_{xx}(n)$ exhibits a steep rise at $|n| \approx 6 \times 10^{12}$ cm^{-2}, which corresponds to full filling of the first superlattice miniband in accord with previous studies on SA TBG [9,14,15]. Three devices with θ of 1.65°, 2.24°, and 2.3°, respectively, were studied—all exhibiting similar transport characteristics (see Supplemental Material [13] for the angle determination procedure).

A notable feature of SA TBG is that, by employing a single- or dual-gated device architecture, one can selectively populate the minivalleys by appropriately tuning the top gate and bottom gate voltages [16,17] (V_{TG} and V_{BG}, respectively). This combination defines the relative

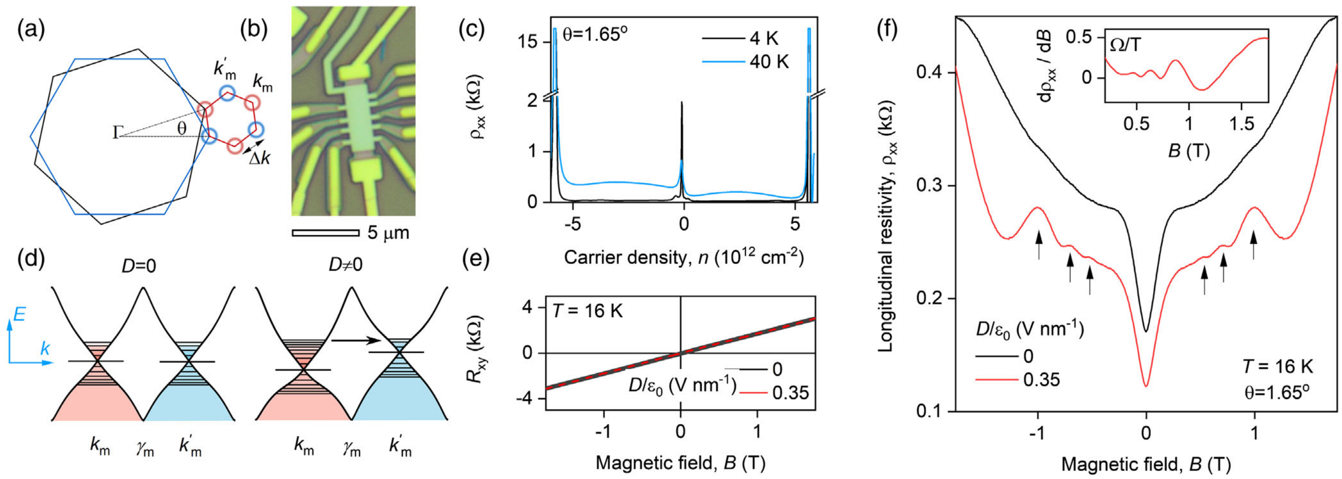

FIG. 1. Interminivalley magneto-oscillations in small-angle twisted bilayer graphene. (a) Schematic illustration of the mini-BZ of the SA TBG superlattice. Red and blue circles represent Fermi surfaces in different minivalleys, labeled k_m and k_m'. (b) Optical photograph of an encapsulated SA TBG device. Yellow, gold contacts; dull green, top gate; light brown, Hall bar mesa. (c) ρ_{xx} as a function of n for the 1.65° device at 4 K (black) and 40 K (blue). $B = 0$, $D = 0$. (d) Calculated single-particle band structure for the 1.65° SA TBG. At low energies two Dirac cones are formed in the vicinity of the k_m and k_m' points. The horizontal black lines represent unevenly spaced LLs that form in the presence of a perpendicular magnetic field. When $D \neq 0$, the cones are shifted with respect to each other. When LLs from different minivalleys get aligned inside the thermal window around the Fermi level, interminivalley scattering (arrow) is enhanced resulting in excess resistivity. (e) Hall resistance R_{xy} as a function of B for two characteristics $D = 0$ and $D/\varepsilon_0 = 0.35$ V/nm yielding $n \approx 0.7 \times 10^{12}$ cm^{-2} measured at $T = 16$ K. (f) ρ_{xx} (symmetrized) as a function of B for the same D, n, and T as in (e). Inset: derivative of the $\rho_{xx}(B)$ dependence for the case of $D/\varepsilon_0 = 0.35$ V/nm.

displacement field between graphene layers, $D = (C_{BG}V_{BG} - C_{TG}V_{TG})/2$, and the total carrier density, $n = (C_{BG}V_{BG} + C_{TG}V_{TG})/e$. Here $C_{TG,BG}$ are the top gate and bottom gate capacitances per unit area, and e is the electron charge. Figure 1(d) shows the calculated band structure of the 1.65° SA TBG for the case of zero and finite D, which clearly demonstrates the gate-induced imbalance in the population between the k_m and k_m' points in the latter case. Intuitively, as the minivalleys are predominantly formed from the energy bands of different graphene sheets, an applied electric field dopes the layers unequally resulting in such an imbalance [16–18]. In the presence of a perpendicular magnetic field B, the gate-induced imbalance also determines the relative offset of the Landau levels (LLs) hosted by each minivalley [19,20], a property that brings us a reliable method to explore the effects of interminivalley electron scattering in SA TBG, as we now proceed to show.

Figure 1(f) compares the magnetoresistance of one of our devices measured at $T = 16$ K for zero and finite $D/\varepsilon_0 = 0.35$ V/nm at the same total n (where ε_0 is the vacuum permittivity). The carrier density was verified via the Hall-effect measurements presented in Fig. 1(e), which shows that the Hall resistance R_{xy} and, therefore, n are identical for both D values. At zero D, ρ_{xx} grows with increasing B but remains featureless: Shubnikov–de Haas oscillations (SdHO) in this device disappear at 15K for this B range [15] (see below). In striking contrast, a clear oscillatory pattern develops in $\rho_{xx}(B)$ data when a finite $D/\varepsilon_0 = 0.35$ V/nm is applied across the graphene layers. The oscillations are even more visible in the derivative of the resistivity with respect to B, $d\rho_{xx}/dB$, [inset in Fig. 1(f)] because of the eliminated magnetoresistance background.

Figure 2(a) details our observations further by comparing the low-field magnetoresistance of another SA TBG device (2.24°) at two characteristics T and $D \neq 0$. At $T = 4.2$ K, ρ_{xx} exhibits the $1/B$-periodic pattern ascribed to SdHO. Because the applied displacement field creates a small difference in the size of the Fermi surfaces associated with the k_m and k_m' minivalleys [see Fig 1(d)], two oscillations of slightly different frequency emerge [14,21,22]. The sum of these produces a familiar beating pattern. At $T > 20$ K, a different oscillation series, characterized by a much lower frequency, dominates the $\rho_{xx}(B)$ behavior. In Fig. 2(b) we plot the amplitude $\Delta\rho_{xx}$ of these oscillations as a function of the inverse magnetic field $1/B$ and demonstrate their $1/B$ periodicity. This periodicity is further verified by plotting the oscillations' extrema indices N against the values of the inverse magnetic field $1/B_N$ at which they appear: all peaks (dips) fall onto straight lines, the slope of which defines the oscillation frequency as $B_0 = \frac{1}{2}\{[d(1/B_N)]/dN\}^{-1}$ [inset of Fig. 2(b)].

Having revealed the $1/B$ character of the high-T resistance oscillations, it is instructive to explore these magneto-oscillations in SA TBG by FFT analysis. As expected from the beating pattern, the FFT spectrum at $T = 4.2$ K is dominated by two closely spaced peaks, labeled as B_1 and B_2 [Fig. 2(c)], containing information on the carrier density in each minivalley $n_{1,2}$ via $B_{1,2} = n_{1,2}h/ge$, where h is

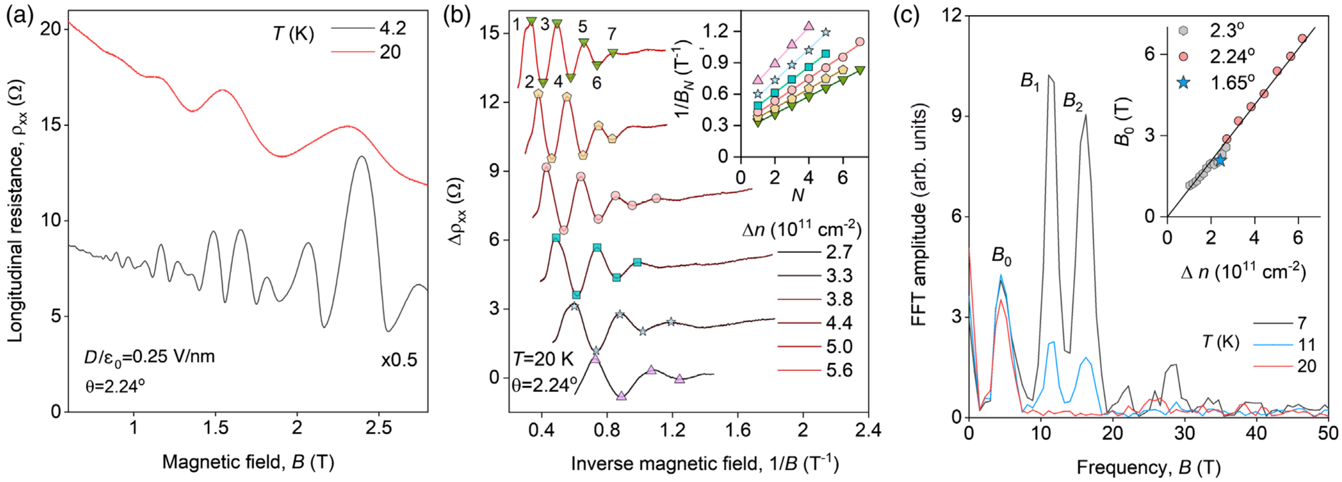

FIG. 2. Fundamental frequency of the interminivalley magneto-oscillations in SA TBG. (a) ρ_{xx} as a function of B for two characteristic $T = 4.2$ and 20 K measured in 2.24° SA TBG. $D/\varepsilon_0 = 0.25$ V/nm, and $n = 2.76 \times 10^{12}$ cm^{-2}. (b) Amplitude of interminivalley magneto-oscillations $\Delta\rho_{xx}$ in our 2.24° device at 20 K after the subtraction of a smooth nonoscillating background. Inset: symbols show resonant values of the inverse magnetic field $1/B_N$ plotted against N for different n corresponding to the matching symbols in (b). Lines: fits to the linear dependence yielding B_0 (see text). (c) Examples of the FFT spectra of the SA TBG magneto-oscillations for characteristic T. B_1 and B_2 determine the SdHO periodicity in different minivalleys, and B_0 is the frequency of interminivalley magneto-oscillations. Inset: B_0 as a function of population imbalance Δn for SA TBG of different angles. Solid line is the expected $B_0 = h\Delta n/4e$ dependence.

Planck's constant and $g = 4$ is the minivalley degeneracy [14]. At $T = 20$ K, the FFT spectrum consists of a single peak at B_0 (labeled accordingly) that matches the periodicity determined from the $1/B_N(N)$ fit [inset of Fig. 2(b)]. Interestingly, the B_0 peak is also visible at $T = 4.2$ and 11K in the FFT spectra, but, because of the complicated beating pattern in $\rho_{xx}(B)$, these oscillations were obscured in previous magnetotransport studies on SA TBG, whereas in large $\theta > 3°$ nonencapsulated devices, they were presumably absent [21]. Critically, we find that the obtained B_0 is identical to the difference $B_2 - B_1$ indicating that the period of the high-T magneto-oscillations is controlled by the carrier density imbalance, $\Delta n = n_2 - n_1$, between the minivalleys (see below).

Figure 3(a) shows the $d\rho_{xx}/dB$ for $\theta = 2.24°$ mapped onto a (B, T) plane. Such representation allows for a convenient illustration of the evolution of magneto-oscillation patterns in SA TBG as a function of T: fast SdHO, clearly visible at liquid helium T, vanish at ~15 K, whereas the slow high-T oscillations persist even above 50 K. We also studied the effect of in plane dc current I_{dc} on magnetoresistance and found that, in contrast to SdHO, which are readily damped by the application of only $I_{dc} \approx 10$ μA because of Joule heating, the amplitude of the high-T magneto-oscillations is resilient to I_{dc}, up to at least 75 μA. Interestingly, we also observed that upon increasing I_{dc}, the phase of these oscillations flips several times, additionally distinguishing them from SdHO (see below and Supplemental Material [13]).

Taken together, the high-T character, peculiar frequency, and fragile phase identify these oscillations as an SA TBG analog of magneto-intersubband oscillations (MISO) discovered in wide quantum wells (QW) and studied in related systems [24–32]. In QW, the oscillations emerge when a two-dimensional electron system (2DES) occupies two or more energy bands capable of electron exchange [24–27,32]. In particular, when the LLs from different subbands become aligned within the thermal window around the Fermi level, elastic interband scattering gives rise to excess resistivity. In the opposite case, when the subbands are misaligned, interband scattering is suppressed. As a result, the resistance experiences $1/B$ periodic oscillations with a period proportional to the difference in the filling factors between the two subbands. In the assumption that the intraband scattering time τ does not depend on the subband index, the oscillations' functional form in the limit of small I_{dc} reads as follows [27,28,32]:

$$\Delta\rho = \frac{2\tau}{\tau_{\text{inter}}}\rho_0\delta_1\delta_2\cos(2\pi\Delta\nu/g). \tag{1}$$

Here ρ_0 is the Drude resistivity, $\delta_{1,2} = \exp(-\pi/\omega_c\tau_{q1,2})$ are the Dingle factors of the two subbands labeled by indices 1 and 2 and expressed in terms of the cyclotron frequency ω_c and the quantum scattering times τ_{q1} and τ_{q2}, g is the subband degeneracy, $\Delta\nu = \nu_2 - \nu_1$ is the difference in filling factors $\nu_{1,2} = n_{1,2}h/Be$ of the subbands, and τ_{inter} is the interband scattering time. Note, while initially derived for 2DES with parabolic spectrum, Eq. (1) becomes generally applicable when expressed in terms of the filling factors. Indeed, $\Delta\nu/g$ universally determines the condition where the LLs in both subbands are aligned. In addition, we

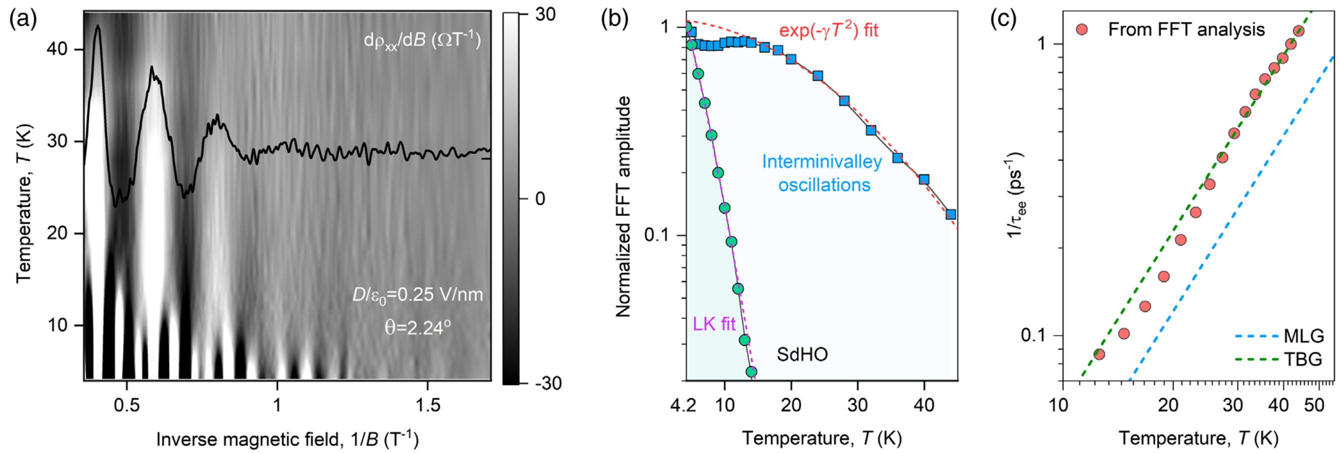

FIG. 3. Temperature dependence of the interminivalley magneto-oscillations in SA TBG. (a) $d\rho_{xx}/dB$ mapped against T and $1/B$ at $n = 2.76 \times 10^{12}$ cm^{-2} and $(D/\varepsilon_0) = 0.25$ V/nm. (b) FFT amplitude of the SdHO and MP oscillations as a function of T. Red dashed line: fit of the high-T region with $\exp(-\gamma T^2)$, where $\gamma = 11.5 \times 10^{-4}$ K^{-2}. Purple dashed line: LK law fit of SdHO. (c) Experimentally derived e-e scattering rate $(1/\tau_{ee})$ versus T (red dots). Blue and green dashed lines are the $1/\tau_{ee}(T)$ dependence for MLG taken from Ref. [23] and the results (green dashed curve) of its renormalization accounting for reduced v_F and eightfold degeneracy in SA TBG at small fillings.

mention that the conditions of our experiments actually correspond to high filling factors and low T where the effects of nonparabolicity and associated nonequidistant LL spectrum are negligible.

To validate the interpretation of the observed high-T magneto-oscillations in SA TBG in the context of MISO physics, we plot the experimentally determined B_0 [from Fig. 2(b)] as a function of Δn in the inset of Fig. 2(b). This difference in carrier density Δn was obtained by a simple electrostatics argument that accounts for the partial screening of the applied field by the graphene layers [17–19] (see Supplemental Material [13]). Additionally, for some D, we also verified the aforementioned Δn values by FFT analysis at liquid helium T as well, where the beating of SdHO can be used to determine Δn. For all our devices, the obtained $B_0(\Delta n)$ dependence was found to be linear over a wide range of Δn and accurately followed the functional form $B_0 = h\Delta n/4e$, where 4 represents the degeneracy of each minivalley. This substantiates the interpretation of the observed oscillations in terms of MISO, where minivalleys now take on the role of the subbands.

Another important characteristic of MISO is its fragile phase with respect to dc bias [33–36]. In the presence of a magnetic field, an electric current I_{dc} of high density generates a substantial Hall field perpendicular to the current flow that initiates additional impurity-assisted tunneling of electrons between the tilted LLs [37–39]. The probability of such tunneling events oscillates with the magnetic field and is maximized when the Hall voltage drop across the cyclotron diameter matches an integer multiple of the cyclotron energy [32]. This leads to the modification of the resonant condition for MISO which manifests itself in multiple phase reversals upon ramping I_{dc}. This interesting behavior was also found in our SA TBG devices, which exhibited the aforementioned phase flips with respect to I_{dc} (see Supplemental Material and Fig. S2 [13]), further supporting the origin of the observed oscillations.

Moreover, unlike SdHO, which also emerge as a result of the Landau quantization, the intersubband oscillations are not sensitive to the smearing of the Fermi distribution, and therefore are damped only through the broadening of LLs, parametrized via the Dingle factors in Eq. (1) [32,34]. Our data reveal this expected behavior too: namely, the FFT amplitude of the interminivalley oscillations features a slow $\exp(-\gamma T^2)$ decay ($\gamma = 11.5 \times 10^{-4}$ K^{-2}), as compared with the relatively fast SdHO thermal damping governed by the conventional Lifshitz-Kosevich (LK) law [dashed purple line in Fig. 3(b)]. This behavior is also consistent with the robustness of the interminivalley oscillations to heating induced by large I_{dc} (see Supplemental Material and Fig. S2 for details [13]).

The observed high-T magneto-oscillations provide a convenient tool to estimate the relative ratio between inter- and intraminivalley scattering rates in SA TBG by fitting them with Eq. (1). From the exponential damping of the oscillations' amplitude with decreasing B, one can extract the quantum scattering time, while ρ_0 can be obtained from the zero-B data leaving $\tau/\tau_{\mathrm{inter}}$ as the only fitting parameter. We have performed such an analysis for our smallest angle device and, from the data shown in Fig. 1(f), found that at $T = 16$ K, τ and τ_{inter} are comparable, indicating the significance of interminivalley scattering processes at small θ (see Supplemental Material and Fig. S3 for details [13]). We also note a drop in the oscillations' amplitude with increasing θ. This indicates the suppression of interminivalley scattering at larger twist angles likely because a larger momentum gain $\sim\Delta k$ is required to initiate such transitions. However, a more accurate comparison on samples with an identical quality is needed to verify such a conclusion.

The interminivalley oscillations also provide an additional insight into the electronic properties of SA TBG: the observed $\exp(-\gamma T^2)$ behavior of the FFT amplitude [Fig. 3(b)] suggests LL broadening induced by e-e scattering [28,32], and thus, its rate $1/\tau_{ee}$ can be conveniently estimated via an analysis of the oscillations' thermal damping [40]. Assuming that this thermal damping is solely encoded in $\delta_1\delta_2$ through the temperature dependence of the quantum scattering times [see Eq. (1)], and that these are identical in both minivalleys (a reasonable assumption when $\Delta n \ll n$) [28], one obtains the T-dependent amplitude of the interminivalley oscillations: $\delta_1\delta_2 = e^{-2\pi/\omega_c\tau_q(T)}$. Since $\tau_q^{-1}(T) = \tau_0^{-1} + \tau_{ee}^{-1}(T)$, where τ_0 is the T-independent elastic quantum scattering time, one can extract τ_{ee}^{-1} from the FFT magnitude of the interminivalley oscillations. Figure 3(c) shows the results of such an analysis and plots the $\tau_{ee}^{-1}(T)$ dependence. For $\theta = 2.24°$, we find that the obtained estimates exceed the e-e scattering rate in MLG [blue dashed curve in Fig. 3(c)] at identical n [23,41,42]. We attribute this enhancement to the reduced $v_F = 0.75v_0$ in the SA TBG of this θ as compared with that of MLG, $v_0 = 10^6$ m/s. Indeed, by renormalizing the $1/\tau_{ee}(T)$ dependence for MLG from Fig. 3(c) by the ratio of the Fermi velocities in these systems and accounting for the twofold increase in the degeneracy of SA TBG as compared with MLG, we obtain the scattering rate for SA TBG, close to that found experimentally.

Our experiments also raise important questions about scattering processes in twisted moiré systems. The observed high-T oscillations indicate the presence of some scattering mechanism(s) enabling electrons to gain enough momentum ($\sim\Delta k$) to escape from their minivalley and scatter to another one ($k_m \leftrightarrow k_m'$). This, in turn, may imply the presence of scatterers with a spatial scale of the order of $1/\Delta k \sim \lambda_m$, where λ_m is the superlattice period. A possible candidate is twist angle disorder, regularly observed in devices fabricated by the methods used here [43]. An alternative scenario involves acoustic phonon-assisted processes [44–46]. However, in our data, the interminivalley oscillations are present even at liquid helium T [Fig. 3(b)], at which the allowed phase space for phonon momenta is not sufficient to ensure the momentum mismatch Δk. At $T = 4.2$ K, phonons with momenta $q < k_B T/\hbar s \approx 4 \times 10^7$ m^{-1} are populated (where $s \approx 20$ km/s is the characteristic speed of sound in graphene), i.e., those having momenta over an order of magnitude smaller than Δk at the studied twist angles. The only phonon branch that at such low T can be populated up to the required momenta is the breathing mode [47]; however, little is known on its impact on SA TBG resistivity [48].

To conclude, we have observed high-T magneto-oscillations in SA TBG when a finite displacement field is applied across the graphene layers. Although similarly periodic in $1/B$, these oscillations show a clearly distinct temperature and dc current dependence from SdHO and are controlled by the difference in the minivalleys' filling factors. Drawing a parallel with MISO, we have shown that the observed oscillations originate from interminivalley scattering, allowed by the reduced size of the mini-Brillouin zone in SA TBG. By analyzing the amplitude of these high-T oscillations, we estimated the relative ratio between interminivalley and intraminivalley scattering times $\tau/\tau_{\mathrm{inter}}$, which we found to be of similar order in the $\theta = 1.65°$ device. Finally, from the temperature dependence of the oscillations, we obtained information on τ_{ee}^{-1}, which we found to exceed that of MLG due to a reduced v_F in this system. Our study points to the presence of a scattering mechanism(s) of unknown nature with large momentum transfer and highlights the importance of interminivalley momentum relaxation in the resistivity of twisted moiré systems [49–53] that has to be accounted for in future studies.

This work was supported by AFOSR Grant No. FA9550-16-1-0382 and the Gordon and Betty Moore Foundation's EPiQS Initiative through Grant No. GBMF9643 to P. J.-H. D. A. B. acknowledges the support from MIT Pappalardo Fellowship. I. Y. P acknowledges support from the MIT undergraduate research opportunities program and the Johnson & Johnson research scholars program. I. A. D. acknowledges support from the German Research Foundation under DFG Projects No. GA501/17-1 (SPP 2244) and No. DM1/5-1. Growth of h-BN crystals was supported by the Elemental Strategy Initiative conducted by the MEXT, Japan, Grants No. JPMXP0112101001, No. JSPS KAKENHI, and No. JP20H00354. We thank Laurence Eaves, Mark Greenaway, Leonid Levitov, Michael Zudov, Volodya Fal'ko, Roshan Krishna Kumar, Vasili Perebeinos, Sergio C. de la Barrera, Alexander A. Zibrov, Alexey Berdyugin, and Mallika Randeria for fruitful discussions.

*bandurin@mit.edu
†pjarillo@mit.edu

[1] Y. Cao, V. Fatemi, S. Fang, K. Watanabe, T. Taniguchi, E. Kaxiras, and P. Jarillo-Herrero, Nature (London) **556**, 43 (2018).

[2] M. Yankowitz, S. Chen, H. Polshyn, Y. Zhang, K. Watanabe, T. Taniguchi, D. Graf, A. F. Young, and C. R. Dean, Science **363**, 1059 (2019).

[3] Y. Cao, V. Fatemi, A. Demir, S. Fang, S. L. Tomarken, J. Y. Luo, J. D. Sanchez-Yamagishi, K. Watanabe, T. Taniguchi, E. Kaxiras, R. C. Ashoori, and P. Jarillo-Herrero, Nature (London) **556**, 80 (2018).

[4] A. L. Sharpe, E. J. Fox, A. W. Barnard, J. Finney, K. Watanabe, T. Taniguchi, M. A. Kastner, and D. Goldhaber-Gordon, Science **365**, 605 (2019).
[5] M. Serlin, C. L. Tschirhart, H. Polshyn, Y. Zhang, J. Zhu, K. Watanabe, T. Taniguchi, L. Balents, and A. F. Young, Science **367**, 900 (2020).
[6] J. M. B. Lopes dos Santos, N. M. R. Peres, and A. H. Castro Neto, Phys. Rev. Lett. **99**, 256802 (2007).
[7] R. Bistritzer and A. H. MacDonald, Proc. Natl. Acad. Sci. U.S.A. **108**, 12233 (2011).
[8] A. H. Castro Neto, F. Guinea, N. M. R. Peres, K. S. Novoselov, and A. K. Geim, Rev. Mod. Phys. **81**, 109 (2009).
[9] K. Kim, A. DaSilva, S. Huang, B. Fallahazad, S. Larentis, T. Taniguchi, K. Watanabe, B. J. LeRoy, A. H. MacDonald, and E. Tutuc, Proc. Natl. Acad. Sci. U.S.A. **114**, 3364 (2017).
[10] J. M. Park, Y. Cao, K. Watanabe, T. Taniguchi, and P. Jarillo-Herrero, arXiv:2008.12296.
[11] D. G. Purdie, N. M. Pugno, T. Taniguchi, K. Watanabe, A. C. Ferrari, and A. Lombardo, Nat. Commun. **9**, 5387 (2018).
[12] M. Ben Shalom, M. J. Zhu, V. I. Fal'ko, A. Mishchenko, A. V. Kretinin, K. S. Novoselov, C. R. Woods, K. Watanabe, T. Taniguchi, A. K. Geim, and J. R. Prance, Nat. Phys. **12**, 318 (2016).
[13] See Supplemental Material at http://link.aps.org/supplemental/10.1103/PhysRevLett.127.056802 for device fabrication details, angle determination procedure, connection between the applied gate voltages and density imbalance, Interminivalley oscillations under strong dc bias, estimating scattering rates ration in SA-TBG.
[14] Y. Kim, P. Herlinger, P. Moon, M. Koshino, T. Taniguchi, K. Watanabe, and J. H. Smet, Nano Lett. **16**, 5053 (2016).
[15] Y. Cao, J. Y. Luo, V. Fatemi, S. Fang, J. D. Sanchez-Yamagishi, K. Watanabe, T. Taniguchi, E. Kaxiras, and P. Jarillo-Herrero, Phys. Rev. Lett. **117**, 116804 (2016).
[16] F. K. de Vries, J. Zhu, E. Portolés, G. Zheng, M. Masseroni, A. Kurzmann, T. Taniguchi, K. Watanabe, A. H. MacDonald, K. Ensslin, T. Ihn, and P. Rickhaus, Phys. Rev. Lett. **125**, 176801 (2020).
[17] A. I. Berdyugin, B. Tsim, P. Kumaravadivel, S. G. Xu, A. Ceferino, A. Knothe, R. K. Kumar, T. Taniguchi, K. Watanabe, A. K. Geim, I. V. Grigorieva, and V. I. Fal'ko, Sci. Adv. **6**, eaay7838 (2020).
[18] S. Slizovskiy, A. Garcia-Ruiz, N. Drummond, and V. I. Falko, arXiv:1912.10067.
[19] J. D. Sanchez-Yamagishi, T. Taychatanapat, K. Watanabe, T. Taniguchi, A. Yacoby, and P. Jarillo-Herrero, Phys. Rev. Lett. **108**, 076601 (2012).
[20] B. Fallahazad, Y. Hao, K. Lee, S. Kim, R. S. Ruoff, and E. Tutuc, Phys. Rev. B **85**, 201408(R) (2012).
[21] H. Schmidt, T. Ldtke, P. Barthold, E. McCann, V. I. Falko, and R. J. Haug, Appl. Phys. Lett. **93**, 172108 (2008).
[22] T.-F. Chung, Y. Xu, and Y. P. Chen, Phys. Rev. B **98**, 035425 (2018).
[23] E. Mönch, D. A. Bandurin, I. A. Dmitriev, I. Y. Phinney, I. Yahniuk, T. Taniguchi, K. Watanabe, P. Jarillo-Herrero, and S. D. Ganichev, Nano Lett. **20**, 5943 (2020).
[24] P. T. Coleridge, Semicond. Sci. Technol. **5**, 961 (1990).
[25] V. Polyanovsky, Fiz. Tekh. Poluprovodn. **12**, 2230 (1988).
[26] D. R. Leadley, R. Fletcher, R. J. Nicholas, F. Tao, C. T. Foxon, and J. J. Harris, Phys. Rev. B **46**, 12439 (1992).
[27] O. E. Raichev, Phys. Rev. B **78**, 125304 (2008).
[28] N. C. Mamani, G. M. Gusev, E. C. F. da Silva, O. E. Raichev, A. A. Quivy, and A. K. Bakarov, Phys. Rev. B **80**, 085304 (2009).
[29] M. V. Kartsovnik, P. D. Grigoriev, W. Biberacher, N. D. Kushch, and P. Wyder, Phys. Rev. Lett. **89**, 126802 (2002).
[30] G. M. Minkov, O. E. Rut, A. A. Sherstobitov, S. A. Dvoretski, N. N. Mikhailov, V. A. Solov'ev, M. Y. Chernov, S. V. Ivanov, and A. V. Germanenko, Phys. Rev. B **101**, 245303 (2020).
[31] S. Abedi, S. A. Vitkalov, A. A. Bykov, and A. K. Bakarov, arXiv:2105.12263.
[32] I. A. Dmitriev, A. D. Mirlin, D. G. Polyakov, and M. A. Zudov, Rev. Mod. Phys. **84**, 1709 (2012).
[33] A. A. Bykov, JETP Lett. **88**, 64 (2008).
[34] N. C. Mamani, G. M. Gusev, O. E. Raichev, T. E. Lamas, and A. K. Bakarov, Phys. Rev. B **80**, 075308 (2009).
[35] S. Wiedmann, G. M. Gusev, O. E. Raichev, A. K. Bakarov, and J. C. Portal, Phys. Rev. B **84**, 165303 (2011).
[36] I. L. Drichko, I. Y. Smirnov, A. K. Bakarov, A. A. Bykov, A. A. Dmitriev, and Y. M. Galperin, JETP Lett. **112**, 45 (2020).
[37] C. L. Yang, J. Zhang, R. R. Du, J. A. Simmons, and J. L. Reno, Phys. Rev. Lett. **89**, 076801 (2002).
[38] M. G. Vavilov, I. L. Aleiner, and L. I. Glazman, Phys. Rev. B **76**, 115331 (2007).
[39] O. E. Raichev and M. A. Zudov, Phys. Rev. Research **2**, 022011(R) (2020).
[40] A. V. Goran, A. A. Bykov, A. I. Toropov, and S. A. Vitkalov, Phys. Rev. B **80**, 193305 (2009).
[41] M. Polini and G. Vignale, arXiv:1404.5728.
[42] R. Krishna Kumar, D. A. Bandurin, F. M. D. Pellegrino, Y. Cao, A. Principi, H. Guo, G. H. Auton, M. Ben Shalom, L. A. Ponomarenko, G. Falkovich, K. Watanabe, T. Taniguchi, I. V. Grigorieva, L. S. Levitov, M. Polini, and A. K. Geim, Nat. Phys. **13**, 1182 (2017).
[43] A. Uri, S. Grover, Y. Cao, J. Crosse, K. Bagani, D. Rodan-Legrain, Y. Myasoedov, K. Watanabe, T. Taniguchi, P. Moon, M. Koshino, P. Jarillo-Herrero, and E. Zeldov, Nature (London) **581**, 47 (2020).
[44] O. E. Raichev, Phys. Rev. B **81**, 195301 (2010).
[45] P. Kumaravadivel, M. T. Greenaway, D. Perello, A. Berdyugin, J. Birkbeck, J. Wengraf, S. Liu, J. H. Edgar, A. K. Geim, L. Eaves, and R. Krishna Kumar, Nat. Commun. **10**, 3334 (2019).
[46] M. T. Greenaway, R. Krishna Kumar, P. Kumaravadivel, A. K. Geim, and L. Eaves, Phys. Rev. B **100**, 155120 (2019).
[47] A. I. Cocemasov, D. L. Nika, and A. A. Balandin, Phys. Rev. B **88**, 035428 (2013).
[48] N. Ray, M. Fleischmann, D. Weckbecker, S. Sharma, O. Pankratov, and S. Shallcross, Phys. Rev. B **94**, 245403 (2016).
[49] T.-F. Chung, Y. Xu, and Y. P. Chen, Phys. Rev. B **98**, 035425 (2018).
[50] H. Polshyn, M. Yankowitz, S. Chen, Y. Zhang, K. Watanabe, T. Taniguchi, C. R. Dean, and A. F. Young, Nat. Phys. **15**, 1011 (2019).

[51] P. Tomi, P. Rickhaus, A. Garcia-Ruiz, G. Zheng, E. Portols, V. Fal'ko, K. Watanabe, T. Taniguchi, K. Ensslin, T. Ihn, and F. K. de Vries, arXiv:2106.07805.

[52] R. Krishna Kumar, X. Chen, G. H. Auton, A. Mishchenko, D. A. Bandurin, S. V. Morozov, Y. Cao, E. Khestanova, M. Ben Shalom, A. V. Kretinin, K. S. Novoselov, L. Eaves, I. V. Grigorieva, L. A. Ponomarenko, V. I. Fal'ko, and A. K. Geim, Science **357**, 181 (2017).

[53] J. R. Wallbank, R. Krishna Kumar, M. Holwill, Z. Wang, G. H. Auton, J. Birkbeck, A. Mishchenko, L. A. Ponomarenko, K. Watanabe, T. Taniguchi, K. S. Novoselov, I. L. Aleiner, A. K. Geim, and V. I. Fal'ko, Nat. Phys. **15**, 32 (2019).